Journal of Materials Chemistry A

ROYAL SOCIETY OF CHEMISTRY

PAPER

View Article Online
View Journal

Cite this: DOI: 10.1039/d1ta11023c

Large-scale cascade cooling performance evaluation of adsorbent/water working pairs by integrated mathematical modelling and machine learning†

Zhilu Liu, [a] Wei Li,[b] Shanshan Cai,[a] Zhengkai Tu, [a] Xiaobing Luo [a] and Song Li *[a]

Efforts to improve the efficiency of adsorption chillers (ACs) catalyzed the invention of cascaded ACs (cACs) with higher overall efficiency that can reutilize the input thermal energy by cascaded stages consisting of a high-temperature stage (HS) and a low-temperature stage (LS). Although the use of water as the refrigerant in cACs is highly attractive, it is an extreme challenging task to identify promising adsorbent/water working pairs from a large number of candidates by a computational or experimental strategy. In this work, the coefficient of performance for cooling (COP_C) and the specific cooling effects (SCE) of over 90 000 cACs based on varying adsorbent/water working pairs were evaluated based on an experimental water adsorption isotherm database (EWAID) by mathematical modelling. Nine cACs with record-breaking COP_C (>1.63) were identified, and it was also revealed that MOFs and zeolites are more potential adsorbents for the HS, while MOFs and COFs are potential candidates for the LS. The relationships between adsorption properties and cooling performance were clearly demonstrated, in which the high water working capacity, I-type water adsorption isotherms with strong adsorbent/water interaction for the HS and V-type adsorption isotherms with the weak interaction for the LS, is favorable for high-performance cACs (*i.e.*, COP_C > 1.5). Besides, the random forest (RF) model of machine learning was successfully executed to accelerate the accurate prediction of the COP_C of thousands of cACs based on adsorbent/water working pairs.

Received 29th December 2021
Accepted 17th March 2022

DOI: 10.1039/d1ta11023c

rsc.li/materials-a

1. Introduction

Thermally driven adsorption chillers (ACs) utilizing solar energy and low-grade waste energy such as engine exhaust or waste heat from industrial processes,[1,2] can be an alternative to the traditional vapor compression refrigeration system, which is beneficial to reducing electricity consumption and alleviating global warming from carbon dioxide emission.[3,4] However, the theoretical upper limit of the coefficient of performance for cooling (COP_C) is only 1 for single-stage ACs consisting of one basic thermodynamic cooling cycle.[5] To further improve the COP_C, advanced AC cycles involving heat and mass recovery, forced convection, multi-bed cascade and so on have been proposed.[4,6–8] Multiple-effect cascaded ACs (cACs) consisting of two or more adsorption beds operating in series can multiply the energy efficiency (COP_C) compared with single-stage ACs, owing to the heat recovery of input thermal energy by cascaded stages at progressively lower temperatures.[9,10] The increased number of cascaded adsorbent beds is able to significantly increase the upper limit of the COP_C, but it also causes an increased driving temperature and the complexity of the device.[11,12] Based on these considerations, cACs including two cooling cycles or two stages (*i.e.* high-temperature stage (HS) and low-temperature stage (LS)) with a theoretical upper limit of $COP_C = 2$ were extensively investigated.[13–15]

The cooling performance of cACs greatly depends on the working pairs including adsorbents and working fluids (*i.e.* refrigerants). As for common working fluids such as water, alcohol, ammonia and alkane, water attracted the most attention due to its abundance, low cost, high enthalpy of evaporation and non-toxicity.[16–18] The cooling performance of traditional adsorbents such as silica gel, zeolite and activated carbon in cACs with water working fluids has been investigated. Douss *et al.* designed and tested a cascading cycle consisting of two zeolite/water beds in the HS and an activated carbon-methanol bed in the LS, which gave rise to a COP_C of 1.06 and a specific cooling power (SCP) of 37 W kg^{-1}.[10] It was reported that the cAC using zeolite/water and silica gel/water

[a]School of Energy and Power Engineering, Huazhong University of Science and Technology, Wuhan 430074, China. E-mail: songli@hust.edu.cn

[b]Energy & Electricity Research Center, Jinan University, Zhuhai 519070, China

† Electronic supplementary information (ESI) available. See DOI: 10.1039/d1ta11023c

working pairs in the HS and LS, respectively, displayed a COP_C of 1.35 that is much higher than that of the single-stage AC (about 0.5).[19] Recently, metal–organic frameworks (MOFs) possessing excellent water adsorption capacity have been regarded as the potential adsorbent candidates for adsorption heat transformation.[20–23] In cACs, the cooling performance of three Zr-based MOFs/water working pairs (*i.e.* NU-1000/water, UiO-66/water and DUT-67/water) in the HS and LS was predicted by mathematical modelling, among which using DUT-67/water working pairs for both the HS and LS achieved the highest COP_C of 1.43 and a circulating cooling capacity of 2.6×10^4 kJ.[24] Rieth *et al.* announced a record-breaking COP_C of 1.63 in cACs with two different MOF/water working pairs (*i.e.* Co_2Cl_2BTDD/water in the HS and Ni_2Cl_2BBTA/water in the LS) at a low driving temperature of 127 °C.[14] In addition, covalent organic frameworks (COFs) also are one kind of potential candidate for cACs.[25,26]

Given the exponentially growing number of possible combinations of working pairs for the LS and HS with the development of adsorbents,[27] especially MOFs,[28] it is impractical to experimentally test the cooling performance of each working pair. High-throughput computational screening (HTCS) based on grand canonical Monte Carlo (GCMC) simulations has been applied to quickly assess the adsorption cooling performance of over three million combinations of MOF/ethanol and COF/ethanol working pairs in cACs, in which small-pore MOFs exhibiting I-type adsorption isotherms and large-pore COFs with stepwise adsorption isotherms are preferential adsorbents for the HS and LS, respectively.[15] However, unlike adsorbent-ethanol, the computational screening of adsorbent/water working pairs by GCCM simulation is extremely challenging mainly due to the ultrahigh computational cost of water adsorption simulation.[29,30] In order to achieve the computational screening of adsorbent/water working pairs of ACs, we constructed an experimental water adsorption isotherm database (EWAID) including hundreds of existing experimental water adsorption isotherms,[31] which enables the large-scale evaluation of the adsorption cooling performance of adsorbent/water working pairs for cACs by mathematical modelling.

Therefore, in this work, the cooling performance of more than 90 000 cACs using adsorbent/water working pairs from the updated EWAID was evaluated by mathematical modelling. The relationships between adsorbent structural properties, adsorption characteristics and cooling performance of working pairs were also explored. Moreover, machine learning (ML) was successfully implemented for quick and precise prediction of the cooling performance of adsorbent/water working pairs.

2. Methods

2.1. Experimental water adsorption isotherm database 2.0

The experimental water adsorption isotherm database (EWAID 1.0) used in our previous work[31] including only 231 adsorbents has been updated to EWAID 2.0 containing 311 adsorbents, in which five MOFs from NIST/ARPA-E database of novel and emerging adsorbent materials[32] and other adsorbents from the latest scientific literature were added. In this work, five types of adsorbents including carbon (Carb), covalent organic frameworks (COFs, C), MOFs (M), porous organic polymers (POPs, P) and zeolites (Z) shown in Table S1† were studied. The experimental water adsorption isotherms of 311 adsorbents were fitted by using the universal adsorption isotherm model (UAIM),[33] and the fitting parameters are provided in Table S3.† In addition, the available structural properties of adsorbents in the database including the accessible surface area (S_a), available pore volume (V_a) and pore diameter (D_p) were also collected from the literature. It should be noted that the pore diameter (D_p) represents the average pore diameter, LCD and dominant pore diameter derived from the pore size distribution reported in the literature, which has been denoted in Tables S2 and S4.† The source literature and detailed structural characteristics can be found in Tables S2 and S4.†

2.2. Cooling performance calculations

Based on the water adsorption isotherms, the adsorption properties including water working capacity (ΔW), heat of adsorption ($\Delta_{ads}H$), isotherm step position (α) and Henry's constant (K_H) can be obtained. ΔW is one of the important factors determining the cooling capacity, which equals the difference of water uptake between adsorption and desorption.[17] $\Delta_{ads}H$ was calculated according to the Clausius–Clapeyron equation.[17] In this work, α reflecting the shape of adsorption curves and K_H describing the affinity between adsorbents and water at ultralow pressure were calculated at 298 K. The definition of α is the relative pressure range corresponding to the largest uptake increment at a given pressure interval ($\Delta(P/P_0) = 0.1$).[31] K_H is the slope of the adsorption isotherm at ultralow water pressure ($P < 31.69$ Pa at 298 K, *i.e.* $P/P_0 = 0$–0.01).[34] The calculated adsorption properties of adsorbents were given in Table S5.†

Two-stage cACs consist of the low-temperature stage (LS) and high-temperature stage (HS). For the ideal isosteric diagram of cACs as shown in Fig. 1, it is assumed that one-kilogram of adsorbents in the HS were desorbed completely, and then all of the heat releasing from the HS was used for the complete

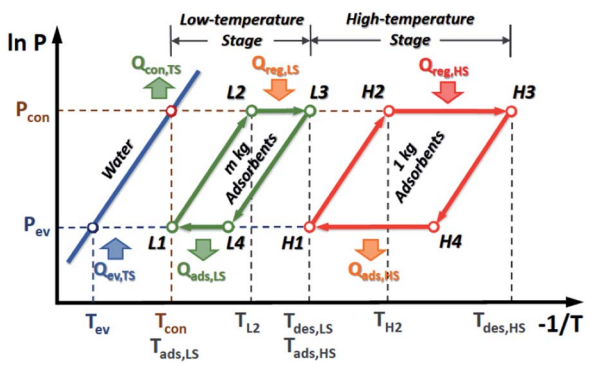

Fig. 1 The ideal isosteric diagram of cascaded adsorption chillers (cACs) consisting of the low-temperature stage (LS, L1–L4) and high-temperature stage (HS, H1–H4). *Q* represents the transferred heat by adsorbent/water working pairs.

regeneration of m-kilogram of adsorbents in the LS (*i.e.* $m = Q'_{reg,HS}/Q'_{reg,LS}$, where Q'_{reg} represents the regeneration energy required for one-kilogram of adsorbents). Therefore, the cooling performance including specific cooling effects and coefficient of performance for cooling in the total system (SCE_{TS} and $COP_{C,TS}$) can be calculated by using eqn (1) and (2):

$$SCE_{TS} = \frac{Q_{ev,TS}}{1+m} = \frac{SCE_{HS} + mSCE_{LS}}{1+m} \quad (1)$$

$$COP_{C,TS} = \frac{Q_{ev,TS}}{Q_{reg,HS}} = COP_{C,HS} + COP_{C,LS} \quad (2)$$

where $Q_{ev,TS}$ represents the transferred heat in the evaporator (cooling capacity) by water working capacity, and $Q_{reg,HS}$ equals the input energy from the external heat source. The SCE and COP of the single-stage ACs can be calculated based on the basic thermodynamic cycle model, and more computational details are described in S2 of the ESI.†

The adopted operational conditions in cACs[14,15] are listed in Table 1. The evaporation temperature (T_{ev}) is the target cooling temperature depending on users' requirements. The condensation temperature (T_{con}) relies on the temperature of the ambient environment. In the LS and HS, the adsorption and desorption temperature (T_{ads} and T_{des}) represent the temperature of the adsorption bed at the end of adsorption and desorption processes, respectively. $T_{ads,LS}$ commonly equals T_{con} depending at ambient temperature, and $T_{des,HS}$ relies on the heat sources. T_{L2} and T_{H2} stand for the initial temperature of the adsorption bed during adsorption processes in the LS and HS, which can be calculated using Trouton's rule.[35] The evaporation pressure (P_{ev}) and condensation pressure (P_{con}) are equal to the saturation pressure of water at T_{ev} and T_{con}, respectively.

2.3. Machine learning

Machine learning (ML) is a more efficient and promising alternative to HTCS based on molecular simulations, which has been employed in the field of gas storage and separation.[36,37] In this work, four ML algorithms including multiple linear regression (MLR), decision tree (DT), gradient boosting machine (GBM) and random forest (RF) were performed to quickly and accurately evaluate the adsorption cooling performance of adsorbent/water working pairs for cACs. Based on four descriptors including the structural characteristics collected from the literature (*i.e.* S_a, V_a and D_p) and Henry's constant (K_H) of adsorbents towards water, the performance of 9025 cACs, which is because the structural information of only 95 adsorbents was experimentally measured and reported, were evaluated by using different ML models, where 80% of samples were randomly chosen as the training dataset and the rest 20% served as the test dataset. The accuracy of each model was assessed using the mean square error (MSE), mean absolute error (MAE) and correlation coefficient (R^2 score). Besides, the relative importance of each descriptor for the HS and LS based on the ML models was also investigated.

Table 1 The operational conditions of each stage in cascaded adsorption heat pumps

Stage	Step	Temperature (K)	Pressure (Pa)
Evaporator	—	$T_{ev} = 283$	$P_{ev} = 1221$
Condenser	—	$T_{con} = 300$	$P_{con} = 3555$
Low-temperature stage (LS)	L1	$T_{ads,LS} = 300$	—
	L2	$T_{L2} = 318$	—
	L3	$T_{des,LS} = 330$	—
High-temperature stage (HS)	H1	$T_{ads,HS} = 330$	—
	H2	$T_{H2} = 352$	—
	H3	$T_{des,HS} = 400$	—

3. Results and discussion

3.1. Cooling performance of adsorbent/water working pairs in cACs

The adsorption cooling performance including $COP_{C,TS}$ and SCE_{TS} of 96 721 cACs based on adsorbent/water working pairs was calculated under given working conditions, and the detailed results are provided in Table S6.† Generally, nine cACs exhibited record-breaking $COP_{C,TS}$ above 1.63,[14] among which the best was the Ni-DOBDC/water working pair in HS + Zr-MOF-808/water working pair in the LS with a $COP_{C,TS}$ of 1.68. The cooling performance of cACs can be classified as 25 categories (adsorbents in HS + adsorbents in LS) shown in Fig. 2. It was found that cACs based on eight classes of adsorbent combinations (*i.e.* MOFs in the HS + carbon, COFs, MOFs, and POPs in the LS; zeolites in the HS + carbon, COFs, MOFs and POPs in the LS) exhibited a higher $COP_{C,TS}$ (*i.e.* $COP_{C,TS} > 1.5$). Besides, it was indicated that MOFs and zeolites are better candidates for the HS, while carbon, COFs, MOFs and POPs are more suitable for the LS. According to Fig. 2 and S2a,† the HS based on zeolite/water showed the highest average $COP_{C,HS}$, leading to an average $COP_{C,TS}$ of around 1. A number of MOFs with high SCE_{HS} exhibited ultrahigh SCE_{TS} (more than 600 kJ kg^{-1}). Moreover, COFs exhibited the highest average $COP_{C,LS}$, followed by MOFs, carbon and POPs (Fig. S2b†), which are potential adsorbent candidates for the LS.

Focusing on high-performance cACs, the number of cACs with high $COP_{C,TS} > 1.5$ based on varying adsorbents in the HS and LS was summarized (Table 2). It was shown that cACs with $COP_{C,TS} > 1.5$ consist of only MOF/water and zeolite/water working pairs in the HS, but mostly COF/water and MOF/water in the LS. Therefore, MOFs and zeolites are more potential candidates for the HS, while MOFs and COFs are promising for the LS. It was also noted that there is a larger number of high-performance MOF/water than other adsorbent/water working pairs in both the HS and LS, which may have resulted from the original large number of MOF samples (around 57% of the total adsorbents) in the database. For cACs with $COP_{C,TS} > 1.5$, the number of MOF/water working pairs in the HS was 0.53% for all cACs consisting of MOF/water in the HS, but 2.13% of the cACs contained zeolite/water in the HS, implicating the higher possibility of zeolite/water as potential working pairs in the HS than MOF/water. 0.73% of cACs with $COP_{C,TS} > 1.5$ were based on COF/water in the LS, while only 0.53% of cACs with $COP_{C,TS} > 1.5$ were based on MOF/water in

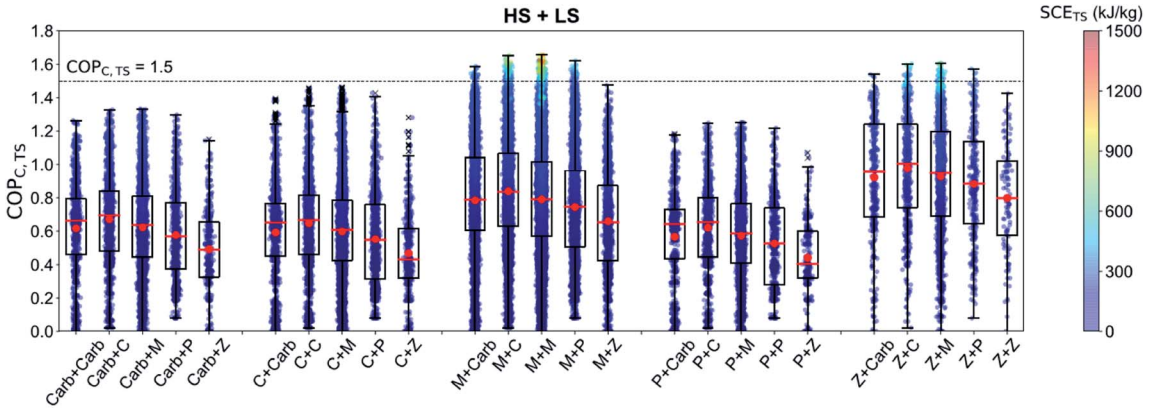

Fig. 2 The cooling performance of 96 721 two-stage cACs based on different adsorbent combinations. $COP_{C,TS}$ and SCE_{TS} are the coefficient of performance for cooling and specific cooling effects of the two-stage (TS) of cACs. The former adsorbent before "+" represents the adsorbent in the high-temperature stage (HS) and the latter is that in the low-temperature stage (LS), among which the five types of adsorbents were included, *i.e.*, carbon (Carb), COFs (C), MOFs (M), POPs (P) and zeolites (Z).

Table 2 The number of cACs with high-performance adsorbents

		Adsorbents no. in HS					Adsorbents no. in LS				
$COP_{C,TS}$ range	cACs no.	Carb	C	M	P	Z	Carb	C	M	P	Z
$COP_{C,TS}$ > 1.5	493	0	0	419	0	73	35	130	291	37	0
$COP_{C,TS}$ > 1.55	205	0	0	182	0	23	6	54	131	14	0
$COP_{C,TS}$ > 1.6	53	0	0	47	0	6	0	13	39	1	0

the LS. Furthermore, it is known that the adsorption cooling performance is mostly dependent on the adsorption properties including water working capacity, the shape of adsorption isotherms and the interaction between adsorbents and the adsorbate.[17,34,38] Therefore, the relationships between adsorption properties and cooling performance of cACs were further explored.

3.2. The relationships between adsorption properties, structural characteristics and cooling performance

Our previous study using the decision tree (DT) model has demonstrated the critical roles of ΔW_{LS} and ΔW_{HS} in determining the COP_C of cACs based on MOF/ethanol and COF/ethanol working pairs.[15] Similarly, the relationship between $COP_{C,TS}$ and the sum of water working capacity of the HS and LS (ΔW_{HS} + ΔW_{LS}) was explored (Fig. 3). It was revealed that $COP_{C,TS}$ increased rapidly with ΔW_{HS} + ΔW_{LS} until a plateau, after which the enhancement in $COP_{C,TS}$ became less significant. It should be noted that no remarkable enhancement of $COP_{C,TS}$ was observed when ΔW_{HS} + ΔW_{LS} > 0.2 kg kg^{-1}. Similar trends were observed in cACs based on ethanol working fluid, in which no remarkable enhancement in $COP_{C,TS}$ was observed when ΔW_{HS} + ΔW_{LS} > 0.4 kg kg^{-1}.[15] Such a difference can be attributed to the discrepancy in the evaporation enthalpy ($\Delta_{vap}H$) of water and ethanol, *i.e.*, the $\Delta_{vap}H$ of water is about twice that of ethanol, suggesting that in order to achieve the same cooling capacity, the amount of water working fluid required is roughly one half that of ethanol.[31] Besides, $COP_{C,TS}$ correlated positively with SCE_{TS}, and thus the high-performance cACs with both high $COP_{C,TS}$ (>1.6) and ultra-high SCE_{TS} (>1000 kJ kg^{-1}) shown in Fig. 3a were identified, all of which are based on MOF/water working pairs such as the cACs based on Co-MOF-74/water[39] and Ni-DOBDC/water[40] in the HS and Co_2Cl_2(-BTDD)/water[41] or Ni_2Cl_2(BTDD)/water[41] in the LS. The high

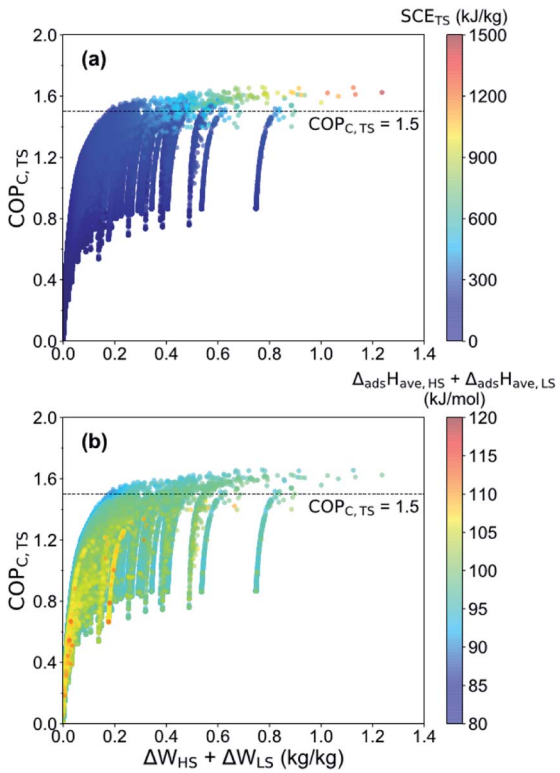

Fig. 3 The relationship between $COP_{C,TS}$ and the summation of water working capacity of the HS (ΔW_{HS}) and LS (ΔW_{LS}). The data points were colored by (a) SCE_{TS} and (b) the summation of average heat of adsorption of the HS ($\Delta_{ads}H_{ave,HS}$) and LS ($\Delta_{ads}H_{ave,LS}$).

water working capacity of these working pairs in the HS (Fig. S3c and d†) contributed the most to their cooling performance. Except for the working capacity, the average heat of adsorption ($\Delta_{ads}H_{ave}$) is another important factor affecting the COP_C. As shown in Fig. 3b, the cACs with a medium $\Delta_{ads}H_{ave,HS}$ + $\Delta_{ads}H_{ave,LS}$ (95–105 mol kg^{-1}) displayed more excellent COP_C at the same ΔW_{HS} + ΔW_{LS}. Besides, the ratio of $\Delta_{ads}H_{ave,HS}$ and $\Delta_{ads}H_{ave,LS}$ is about 0.9–1.2 for cACs with high $COP_{C,TS}$, indicating that similar $\Delta_{ads}H_{ave}$ of the HS and LS in the range of 45–52.5 kJ mol^{-1} is favorable for cooling performance (Fig. S4†).

Henry's constant (K_H) describing the interaction between the adsorbent and adsorbate at ultralow pressure also implicates the hydrophilicity and hydrophobicity of adsorbents.[34] The results shown in Fig. 4 indicate the impact of K_H of adsorbents in the HS and LS on $COP_{C,TS}$ of cACs. The ratio of $K_{H,HS}$ and $K_{H,LS}$ ($K_{H,HS}/K_{H,LS}$) in the range of 10^0–10^9 was observed in high-performance cACs ($COP_{C,TS}$ > 1.5) with $K_{H,HS}$ = 10^{-3}–10^0 mol (kg^{-1} Pa^{-1}), suggesting that the more hydrophilic adsorbents in the HS are favorable for $COP_{C,TS}$ of cACs. The positive relationship between COP_C and K_H and the optimal range of K_H for high-performance cACs (*i.e.*, 10^{-3} < $K_{H,HS}$ < 10^0 for $COP_{C,HS}$ > 0.7, and 10^{-7} < $K_{H,LS}$ < 10^{-1} for $COP_{C,LS}$ > 0.8) are shown in Fig. S5.† Besides, the negative correlation between K_H and the step position (α) was observed,[34] in which the outstanding adsorbents in the HS with high K_H usually exhibited a smaller α, while potential adsorbents in the LS exhibited a larger α. Subsequently, the optimum step position or the adsorption isotherm shape of adsorbents for the HS and LS was explored, respectively.

The number of adsorbents with different step positions (α) at 298 K is summarized in Table S7.† Fig. 5 displays COP_C and step position (α) of 311 adsorbent/water working pairs, respectively. In the HS, adsorbents with 0 < α < 0.1 showed the highest average $COP_{C,HS}$, which commonly corresponds to I-type adsorption isotherms, indicating the hydrophilicity of stronger interaction between adsorbents and water. In the LS, adsorbents with 0.2 < α < 0.4 showed a higher $COP_{C,LS}$,

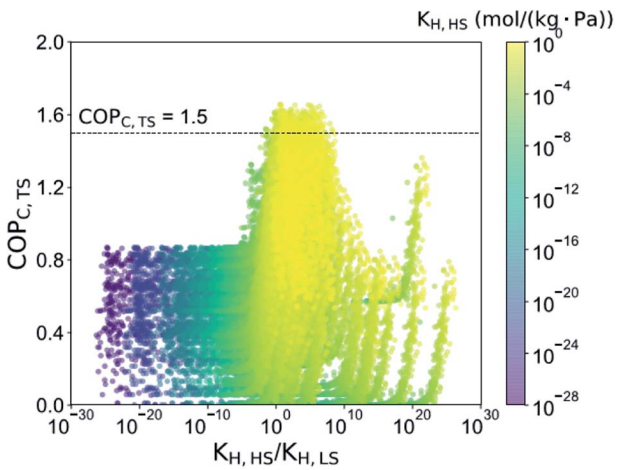

Fig. 4 The relationship between $COP_{C,TS}$ and the ratio of Henry's constant of the high-temperature stage (HS) and low-temperature stage (LS) ($K_{H,HS}/K_{H,LS}$).

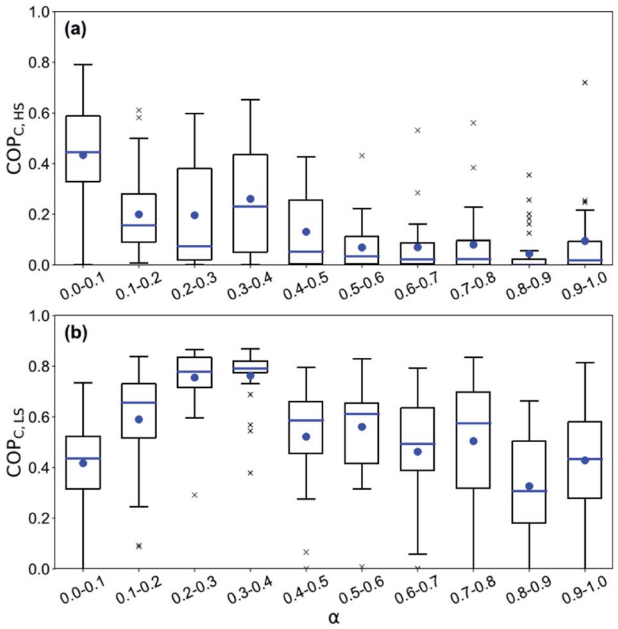

Fig. 5 COP_C and step position (α) of 311 adsorbent/water working pairs in (a) high-temperature stage (HS) and (b) low-temperature stage (LS).

corresponding to the V-type (or "S" shaped) isotherm and the hydrophobicity of adsorbents or weaker adsorbent/water interaction. Such tendencies are in line with the correlation between the $COP_{C,TS}$ and $K_{H,HS}/K_{H,LS}$ ratio. In addition, the high-performance adsorbents in the HS were identified as MOFs and zeolites with 0 < α < 0.2 (Fig. S6†), and the average $COP_{C,HS}$ of zeolites is generally higher than that of MOFs due to the fact that most of the zeolites (~80%) exhibit 0 < α < 0.1. However, the high-performance adsorbents in the LS (*i.e.*, $COP_{C,LS}$ > 0.7) were MOFs and COFs with 0.2 < α < 0.4.

The correlation between structural characteristics and cooling performance shown in Fig. S7† demonstrates that the high-performance adsorbents of the HS exhibit an accessible surface area (S_a) of 500–1500 m^2 g^{-1}, available pore volume (V_a) of approximately 0.5 cm^3/and pore size (D_p) of 12 Å, respectively. In comparison, the top performers for the LS exhibit a wide-range of structural characteristics. It may be ascribed to the larger number of high-performance adsorbents for the LS, which is resulted from more adsorbents in the database exhibiting low Henry's constant (Fig. S5†) or high step position (α) (Fig. S6†) that is favorable for $COP_{C,LS}$. It should be noted that with increasing adsorbent number and structural diversity of the database, a strong correlation between structural characteristics of adsorbents and cooling performance may be observed, which can provide more helpful insights into the designing of potential adsorbents for cACs using water as the working fluid.

According to the selected top 10 adsorbents with the highest $COP_{C,HS}$ and $COP_{C,LS}$ shown in Tables S8 and S9,† respectively, it was found that the top performers of the HS generally exhibited higher K_H and lower α than those of the LS, leading to lower ΔW and $COP_{C,HS}$ than $COP_{C,LS}$, which is consistent with previous observations. Since most of the top performers are

MOFs in both the HS and LS, water stability is still a concern. Among the 8 MOFs of top 10 performers of the HS, only two MOFs, *i.e.* Ni-DOBDC[40] and CPO-27-Ni[42] exhibit decent water stability, which may have resulted from the hydrophilic nature of selected candidates. However, nearly all MOFs in top 10 performers of the LS are water stable, which may be ascribed to the hydrophobic nature of selected adsorbents that is favorable for $COP_{C,LS}$. It is also noticed that some well-known MOFs were identified from screening. For example, MIL-100(Fe)[43] and Co_2Cl_2(BTDD)[41] perform well in both the HS and LS with high water stability. Al-based MOFs with excellent water cycling stability and potentials in thermal conversion application[44–46] were also noticed. MIL-160(Al)[47] was identified as a potential candidate for the HS with a $COP_{C,HS}$ of 0.62, whereas CAU-23(Al)[45] was recognized as a potential candidate for the LS with a $COP_{C,LS}$ of 0.86. The development of green syntheses and large-scale production of MOFs may enable their industrial application in future.[48–51]

3.3. Machine learning

Machine learning (ML) models can be an effective alternative to time-consuming HTCS. In this study, four ML models including MLR, GBM, DT and RF were carried out for predicting the $COP_{C,TS}$ of cACs, in which three structural characteristics (*i.e.* S_a, V_a and D_p) and K_H of adsorbents in the HS and LS were adopted as descriptors, respectively. The prediction results of ML models with 80% samples used for training and the rest 20% for testing are shown in Table 3. Among the four models, the RF model performed the best with the lowest MSE, mean absolute error (MAE) and highest correlation coefficient (R^2 score).

According to Fig. 6a and S8,† RF gave rise to the highest prediction accuracy ($R^2 = 0.93$), followed by GBM ($R^2 = 0.92$), DT ($R^2 = 0.91$) and MLR ($R^2 = 0.16$). Distinctly, the nonlinear ML models perform better than linear MLR, which may be ascribed to the complicated correlation between descriptors and COP_C that cannot be accurately described by linear models. Besides, the polarity of water molecules and their hydrogen bond network formed may contribute to the complexity of correlation between structural/chemical properties, water uptake and COP_C. The relative importance of descriptors of adsorbents in the HS and LS was also obtained by RF (Fig. 6b). The results demonstrated that K_H contributed the most, *i.e.*, 47% relative importance of the HS and 22% of the LS for $COP_{C,TS}$ prediction, indicating the key role

Table 3 $COP_{C,TS}$ prediction accuracy by using different machine learning (ML) models

ML models	MSE[a]	MAE[a]	R^2 score[a]
MLR	0.096	0.247	0.16
DT	0.010	0.067	0.91
GBM	0.010	0.063	0.92
RF	0.009	0.063	0.93

[a] Mean square error (MSE), mean absolute error (MAE) and correlation coefficient (R^2 score) are the evaluation indexes based on the total dataset.

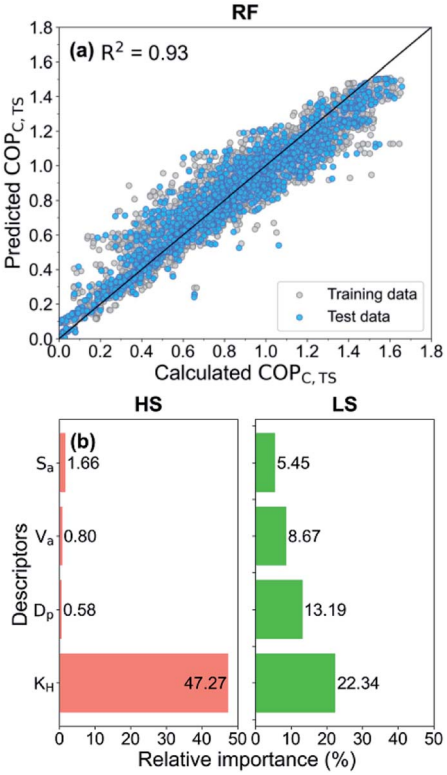

Fig. 6 (a) $COP_{C,TS}$ predicted by using the random forest (RF) model. (b) The relative importance of different descriptors (*i.e.* accessible surface area (S_a), available pore volume (V_a), pore diameter (D_p) and Henry's constant (K_H) of the working pair in the HS and LS) from the RF model for $COP_{C,TS}$ prediction.

of hydrophilicity of adsorbents or the shape of adsorption isotherm in determining the cooling performance in cACs. Specifically, the stronger adsorbent/water interaction leading to I-type isotherms is favorable for the HS, and the weaker interaction corresponding to V-type isotherms is beneficial to the LS. In addition, the relative importance of structural characteristics in the LS is higher than that in the HS, which may be ascribed to the relatively higher working capacity of most adsorbents in the LS than those of the HS that imposes remarkable impacts on COP_C (Fig. S7†). Such a phenomenon may also correlate with the larger number of adsorbents with favorable K_H for the LS. Moreover, the impacts of the training dataset size on the prediction accuracy (R^2) by RF and other models were displayed (Fig. S9†). As for the RF model, a prediction accuracy of $R^2 > 0.9$ could be achieved by using more than 60% samples as the training dataset, and a higher prediction accuracy of $R^2 > 0.8$ could be reached with 30% samples as the training dataset. Besides, RF models is able to accurately predict the $COP_{C,TS}$ of cACs within several seconds, which could be a fast and effective tool to identify top performers for cACs from a large number of adsorbent/water working pairs.

4. Conclusions

In this work, we evaluated the cooling performance of more than 90 000 cACs based on adsorbent/water working pairs using the experimental water adsorption isotherm database (EWAID)

by mathematical modelling and machine learning. We found nine cACs with record-breaking COP_C (>1.63), and MOFs and zeolites are better candidates for the HS, while MOFs and COFs are more promising candidates for the LS. The high-performance cACs with $COP_{C,TS} > 1.5$ exhibited $\Delta W_{HS} + \Delta W_{LS} > 0.2$ kg kg^{-1}, $\Delta_{ads}H_{ave,HS} + \Delta_{ads}H_{ave,LS} = 95$–$105$ kJ mol^{-1}, and $K_{H,HS}/K_{H,LS} = 10^0$–10^9 with $K_{H,HS} = 10^{-3}$–10^0 mol (kg^{-1} Pa^{-1}), $0 < \alpha < 0.1$ for the HS and $0.2 < \alpha < 0.4$ for the LS, respectively. The results indicated that high-performance adsorbents should exhibit a high working capacity in both the HS and LS, I-type water adsorption isotherms with strong adsorbent/water interaction for the HS, while V-type adsorption isotherms with the weak adsorbent/water interaction for the LS. Moreover, four machine learning models were used for quickly predicting the cooling performance of a large number of cACs. The random forest (RF) model outperformed other models with $R^2 = 0.93$, in which the hydrophilicity (*i.e.* K_H) of adsorbents in the HS and LS plays the key role in determining the cooling performance of cACs based on water working fluid. The evaluation approaches based on the EWAID in this work can accelerate the discovery of the high-performance working pairs for cACs, which may be extended to other energy storage and conversion systems in the future.

Conflicts of interest

There are no conflicts to declare.

Acknowledgements

This work was supported by National Key Research and Development Program of China (No. 2020YFB1506300). The computation was carried out at National Supercomputer Center in Shenzhen.

Notes and references

1 P. Cunningham, *Cogener. Distrib. Gener. J.*, 2002, **17**, 31–51.
2 R. Z. Wang, Z. Z. Xia, L. W. Wang, Z. S. Lu, S. L. Li, T. X. Li, J. Y. Wu and S. He, *Energy*, 2011, **36**, 5425–5439.
3 M. A. Lambert and B. J. Jones, *J. Thermophys. Heat Transfer*, 2005, **19**, 471–485.
4 F. Meunier, *Appl. Therm. Eng.*, 2013, **61**, 830–836.
5 V. E. Sharonov and Y. I. Aristov, *Chem. Eng. J.*, 2008, **136**, 419–424.
6 X. H. Li, X. H. Hou, X. Zhang and Z. X. Yuan, *Energy Convers. Manage.*, 2015, **94**, 221–232.
7 S. Ye, B. Xue, X. Meng, X. Wei, K. Nakaso and J. Fukai, *Sustain. Cities Soc.*, 2020, **52**, 101808.
8 C. Olkis, S. Brandani and G. Santori, *Chem. Eng. J.*, 2019, **378**, 122104.
9 F. Meunier, *J. Heat Recovery Syst.*, 1986, **6**, 491–498.
10 N. Douss and F. Meunier, *Chem. Eng. Sci.*, 1989, **44**, 225–235.
11 B. B. Saha and T. Kashiwagi, *ASHRAE Trans.*, 1997, **103**, 50.
12 Q. Pan, R. Wang, N. Vorayos and T. Kiatsiriroat, *Int. J. Refrig.*, 2018, **95**, 21–27.
13 F. Meunier, *J. Heat Recovery Syst.*, 1985, **5**, 133–141.
14 A. J. Rieth, A. M. Wright, S. Rao, H. Kim, A. D. LaPotin, E. N. Wang and M. Dincă, *J. Am. Chem. Soc.*, 2018, **140**, 17591–17596.
15 W. Li, X. Xia and S. Li, *J. Mater. Chem. A*, 2019, **7**, 25010–25019.
16 R. E. Critoph and Y. Zhong, *Proc. Inst. Mech. Eng., Part E*, 2005, **219**, 285–300.
17 M. F. d. Lange, K. J. F. M. Verouden, T. J. H. Vlugt, J. Gascon and F. Kapteijn, *Chem. Rev.*, 2015, **115**, 12205–12250.
18 H. J. An, M. Sarker, D. K. Yoo and S. H. Jhung, *Chem. Eng. J.*, 2019, **373**, 1064–1071.
19 Y. Liu and K. C. Leong, *Int. J. Refrig.*, 2006, **29**, 250–259.
20 D. M. Steinert, S. J. Ernst, S. K. Henninger and C. Janiak, *Eur. J. Inorg. Chem.*, 2020, **2020**, 4502–4515.
21 C. Janiak and S. K. Henninger, *Chimia*, 2013, **67**, 419–424.
22 X. Liu, X. Wang and F. Kapteijn, *Chem. Rev.*, 2020, **120**, 8303–8377.
23 L. G. Gordeeva, Y. D. Tu, Q. Pan, M. L. Palash, B. B. Saha, Y. I. Aristov and R. Z. Wang, *Nano Energy*, 2021, **84**, 105946.
24 S. Wang, X. Xia and S. Li, *Appl. Therm. Eng.*, 2021, **189**, 116707.
25 J. Perez-Carvajal, G. Boix, I. Imaz and D. Maspoch, *Adv. Energy Mater.*, 2019, **9**, 5.
26 X. Xia, Z. Liu and S. Li, *Appl. Therm. Eng.*, 2020, **176**, 115442.
27 Y. I. Aristov, *Appl. Therm. Eng.*, 2013, **50**, 1610–1618.
28 H. Daglar and S. Keskin, *Coord. Chem. Rev.*, 2020, **422**, 20.
29 Y. J. Colón and R. Q. Snurr, *Chem. Soc. Rev.*, 2014, **43**, 5735–5749.
30 Z. Liu, W. Li, H. Liu, X. Zhuang and S. Li, *Acta Chim. Sin.*, 2019, **77**, 323–339.
31 Z. Liu, W. Li, P. Z. Moghadam and S. Li, *Sustainable Energy Fuels*, 2021, **5**, 1075–1084.
32 *NIST/ARPA-E Database of Novel and Emerging Adsorbent Materials*, https://adsorbents.nist.gov/isodb/index.php#home.
33 K. C. Ng, M. Burhan, M. W. Shahzad and A. B. Ismail, *Sci. Rep.*, 2017, **7**, 10634.
34 J. Canivet, J. Bonnefoy, C. Daniel, A. Legrand, B. Coasne and D. Farrusseng, *New J. Chem.*, 2014, **38**, 3102–3111.
35 Y. I. Aristov, M. M. Tokarev and V. E. Sharonov, *Chem. Eng. Sci.*, 2008, **63**, 2907–2912.
36 S. Chong, S. Lee, B. Kim and J. Kim, *Coord. Chem. Rev.*, 2020, **423**, 213487.
37 Z. Shi, W. Yang, X. Deng, C. Cai, Y. Yan, H. Liang, Z. Liu and Z. Qiao, *Mol. Syst. Des. Eng.*, 2020, **5**, 725–742.
38 W. Li, X. Xia, M. Cao and S. Li, *J. Mater. Chem. A*, 2019, **7**, 7470–7479.
39 H.-Y. Cho, D.-A. Yang, J. Kim, S.-Y. Jeong and W.-S. Ahn, *Catal. Today*, 2012, **185**, 35–40.
40 J. Liu, Y. Wang, A. I. Benin, P. Jakubczak, R. R. Willis and M. D. LeVan, *Langmuir*, 2010, **26**, 14301–14307.
41 A. J. Rieth, S. Yang, E. N. Wang and M. Dinca, *ACS Cent. Sci.*, 2017, **3**, 668–672.
42 A. Das, P. D. Southon, M. Zhao, C. J. Kepert, A. T. Harris and D. M. D'Alessandro, *Dalton Trans.*, 2012, **41**, 11739–11744.
43 P. Küsgens, M. Rose, I. Senkovska, H. Fröde, A. Henschel, S. Siegle and S. Kaskel, *Microporous Mesoporous Mater.*, 2009, **120**, 325–330.

44 A. Permyakova, O. Skrylnyk, E. Courbon, M. Affram, S. Wang, U. H. Lee, A. H. Valekar, F. Nouar, G. Mouchaham and T. Devic, *ChemSusChem*, 2017, **10**, 1419–1426.
45 D. Lenzen, J. Zhao, S. J. Ernst, M. Wahiduzzaman, A. Ken Inge, D. Frohlich, H. Xu, H. J. Bart, C. Janiak, S. Henninger, G. Maurin, X. Zou and N. Stock, *Nat. Commun.*, 2019, **10**, 3025.
46 N. Tannert, S.-J. Ernst, C. Jansen, H.-J. Bart, S. K. Henninger and C. Janiak, *J. Mater. Chem. A*, 2018, **6**, 17706–17712.
47 A. Cadiau, J. S. Lee, D. Damasceno Borges, P. Fabry, T. Devic, M. T. Wharmby, C. Martineau, D. Foucher, F. Taulelle, C. H. Jun, Y. K. Hwang, N. Stock, M. F. De Lange, F. Kapteijn, J. Gascon, G. Maurin, J. S. Chang and C. Serre, *Adv. Mater.*, 2015, **27**, 4775–4780.
48 D. Lenzen, P. Bendix, H. Reinsch, D. Frohlich, H. Kummer, M. Mollers, P. P. C. Hugenell, R. Glaser, S. Henninger and N. Stock, *Adv. Mater.*, 2018, **30**, 1705869.
49 J. Ren, X. Dyosiba, N. M. Musyoka, H. W. Langmi, M. Mathe and S. Liao, *Coord. Chem. Rev.*, 2017, **352**, 187–219.
50 P. A. Julien, C. Mottillo and T. Friščić, *Green Chem.*, 2017, **19**, 2729–2747.
51 S. Kumar, S. Jain, M. Nehra, N. Dilbaghi, G. Marrazza and K.-H. Kim, *Coord. Chem. Rev.*, 2020, **420**, 213407.

